DOI: 10.1002/ ((please add manuscript number))
Article type: Full Paper

Single-cell biodetection by upconverting microspinners

Elisa Ortiz-Rivero, Katarzyna Prorok, Michal Skowicki, Dasheng Lu, Artur Bednarkiewicz, Daniel Jaque* and Patricia Haro-González.*

E. Ortiz-Rivero, D. Lu, Prof. D. Jaque, Dr. P. Haro-González
Fluorescence Imaging Group, Departamento de Física de Materiales, Facultad de Ciencias, Universidad Autónoma de Madrid, 28049, Spain
E-mail: daniel.jaque@uam.es

Dr. K. Prorok, Prof. Artur Bednarkiewicz
Institute of Low Temperature and Structure Research, Polish Academy of Sciences, ul.Okolna 2, 50-422 Wroclaw, Poland
E-mail: a.bednarkiewicz@intibs.pl

Dr. Michal Skowicki
Łukasiewicz Research Network – Port Polish center for Technology Development, ul.Stablowicka 147, 54-066 Wrocław, Poland

Prof. D. Jaque
Nanobiology Group, Instituto Ramón y Cajal de Investigación, Sanitaria Hospital Ramón y Cajal, Ctra.De Colmenar Viejo, Km. 9100, 28034 Madrid, Spain

Keywords: spinner, upconversion, optical trapping, bacteria, candida cell

Abstract

Near-infrared-light-mediated optical tweezing of individual upconverting particles has enabled all-optical single-cell studies, such as intracellular thermal sensing and minimally invasive cytoplasm investigations. Furthermore, the intrinsic optical birefringence of upconverting particles renders them light-driven luminescent spinners with a yet unexplored potential in biomedicine. In this work, we showcase the use of upconverting spinners for the accurate and specific detection of single-cell and single-bacteria attachment events, through real-time monitoring of rotation velocity. The physical mechanisms linking single-attachment to the angular deceleration of upconverting spinners are discussed in detail. Concomitantly, the upconversion emission generated by the spinner is harnessed for simultaneous thermal sensing and thermal control during the attachment event. Results here included demonstrate the potential of upconverting particles for the development of fast, high-sensitivity and cost-effective systems for single-cell biodetection.

1. Introduction

Single-body (eukaryotic cell or bacteria) detection is nowadays required by a large number of disciplines ranging from food safety, environmental monitoring, pharmaceutical industry and biomedicine. [1] Such detection should be done in a contactless way to reduce the risk of contamination while keeping the perturbation of the measured system at minimum. In the case of a bacterium, its single-body detection in bio-fluids (such as urine and blood), food or drinking water, would constitute the first step towards early quantitative diagnosis of different infections. This, in turn, would allow their treatment at the early stage, increasing the success probability by, for instance, adjusting the antibiotic treatment to counter fight the specific infection. On the other hand, single-cell detection would be of great interest in the diagnosis of other serious systemic fungal infections like candidiasis (by e.g. *Candida albicans*) or metastatic processes that lead to the presence of circulating cancer cells in the bloodstream.[2] Detection of such cells in blood samples would indicate an elevated risk of infections or metastasis, respectively, and would help clinicians to adopt adequate treatments.

Nowadays, bacteria and cell detection in biological fluids is being achieved by "massive" approaches that are far from being able to detect single cells or bacteria. For instance, traditional approaches for bacteria detection are based on an enrichment step to increase the number of bacteria in the sample under study to reach a certain detection level.[3] These methods require a substantial amount of time (typically more than 24 hours) and are only applicable when the initial concentration of bacteria in the "seed sample" is larger than a threshold value. On the other hand, the presence of "anomalous" cancer cells in blood samples is nowadays detected by conventional hematology analyzers that require large amount of cells to provide a reliable readout.[4] Therefore, the existing challenge is

to develop rapid, sensitive, and specific methods that are capable of simultaneously detecting both bacteria and cells at the single-body level.[5]

To enhance the sensitivity and detection speed of the above described approaches, a number of immunoassays have been developed based on bioconjugated nanoparticles, kinetic exclusion assays and on-chip microfluidic platforms.[6] Nevertheless, most of these methods need sophisticated instrumentation, which makes the process expensive. They also imply complex sample manipulation and relative large response times. Bio-photonics has emerged as a possible alternative to traditional methods. Indeed, a variety of optical methods has been developed based on spectroscopy and microscopy approaches that exploit the light-matter interaction. [6a, 6b] In this context, different types of inorganic micro- and nano-particles (such as lanthanide, gold and silver based particles) have raised great expectations over the traditional organic fluorophores because their attractive optical and chemical features.[7] Some of them are high photostable, exhibit, easily tunable spectral properties, multiplexed (i.e. a few targets in the same sample) and multimode (e.g. fluorescence+MRI) detection and lack of induction of autofluorescence.[5b, 5c, 8] Among the different particles used in biophotonics, Upconverting Particles (UCPs) have attracted great attention. UCPs are capable of infrared-to-visible optical conversion through sequential multistep absorption of infrared photons.[9] This makes possible the acquisition of high resolution and low background bio-images.[10] UCPs have been also widely used for intracellular biosensing thanks to their bright, background-free and temperature dependent luminescence.[11] However, most of these demonstrations exploited passive diffusion of nanoparticles and simple labeling of biological samples with no or limited bio-sensing reporting capability, while intentional manipulation of such responsive ‘sensors’ could be a valuable possibility for development of future single-body biosensors.

Optical trapping has emerged as a reliable technique to achieve precise translation and rotational control over micro- and nano-structures.[12] It is a contactless technique that has been already used for long-term studies of single cells and bacteria.[13] Very recently, it has been demonstrated how single laser beams can not only trap but also induce rotation of birefringent UCPs.[14] The rotation dynamics of these "upconverting Spinners" (UCSPNs) has been found to be strongly dependent on the rotating mass and environmental conditions (e.g. viscosity, temperature, etc..) so that they have been introduced to the scientific community as a potential high-sensitivity biosensors. Nevertheless, despite these promising results, the use of optically driven UCSPNs as biosensors has remained unexplored so far.

In this work, we have used UCSPNs for contactless detection of single bacteria and opportunistic pathogenic yeast cells. Single-body detection is achieved by real time monitoring of the rotation dynamics of a hexagonal ytterbium and erbium codoped $NaYF_4$ microparticle. By using surface functionalized with an adequate biomolecule, a single bacteria or cell adhesion is evidenced by an angular deceleration that can be monitored in real time by a straightforward analysis of either the transmitted laser beam or of the visible luminescence generated by UCSPNs. Control experiments carried out with non-functionalized UCSPNs have been also performed to evidence the selectivity of the method here proposed. Finally, simple calculations are presented to elucidate the dominating mechanism at the basis of the single-body induced change in rotation dynamics.

2. Results and discussion

2.1. Optical and morphological characterization of Upconverting Spinners.

Birefringent upconverting microparticles ($NaYF_4$:Er,Yb), synthetized as described in Supporting Information, present hexagonal shape with average diameter and thickness of 4.4 ± 0.3 μm and 1.4 ± 0.2 μm, respectively (see **Figure 1a**). Previous studies demonstrated that their optical (extraordinary) axis points parallel to the shortest dimension (i.e. perpendicularly to the hexagonal faces) whereas the two orthogonal ordinary axis are both contained in the hexagonal plane. [15] The $NaYF_4$:Er,Yb microparticles used here, show an intense visible emission when optically excited by either 800 or 980 nm radiation thanks to a multiphoton excitation process already described elsewhere.[16] The upconverting emission spectra generated by the $NaYF_4$:Er,Yb microspinners is included in Supporting Information. The visible emission spectra generated by our $NaYF_4$:Er,Yb UCSPNs is highly polarized and shows a remarkable temperature dependence.[17] This combination allows, based on a straightforward analysis of the upconverting luminescence, for real time and contactless thermal sensing as well as for an accurate determination of $NaYF_4$:Er,Yb UCSPN position and orientation.[18] In order to provide $NaYF_4$:Er,Yb microspinners with selective adhesion to bacteria and cells they were surface decorated with Protein G (Supporting information S2).[19] The existence of the protein coating at the surface of $NaYF_4$:Er,Yb UCSPNs is evidenced by the Fourier-transform infrared (FTIR) spectrum shown in **Figure 1b**. The split peaks at 1630 and 1582 cm^{-1} are due to the stretch of the C=O bond, characteristic of the polypeptides. **Figure 1c** shows, in a schematic way, the surface decoration process (described in Supporting Information), which is responsible for providing the $NaYF_4$:Er,Yb microspinners with selective binding functions.

2.2. Optical rotation of upconverting microspinners: Principle of detection.

For optically induced rotation of $NaYF_4$:Er,Yb microspinners, the optical system schematically represented in **Figure 2a** was used. A linearly polarized 790 nm, single-mode, fiber coupled diode laser was used as optical excitation source. A quarter-wave plate placed afterwards converted the laser beam into circularly polarized light. Optical excitation at 790 nm was selected as it keeps at minimum the laser induced thermal loading of the microspinner and surrounding medium. An aqueous solution of $NaYF_4$:Er,Yb UCSPNs was placed into a 120 μm height micro-chamber (more experimental details are given in Supporting Information S3). The circularly polarized 790 nm radiation provided by the diode laser was focused into the chamber containing the $NaYF_4$:Er,Yb microspinners by using a 100X microscope objective with a Numerical Aperture of 0.85 that leads to a spot size of 1.2 μm. In this experimental conditions, a single $NaYF_4$:Er,Yb UCSPN can be, simultaneously, optically trapped and rotated. Real time observation of $NaYF_4$:Er,Yb microspinners was achieved by using a CCD camera coupled to the system together with a set of different spectral filters used to remove the laser light (see **Figure 2b**). A quadrant photodiode detects the laser light transmitted/scattered by the $NaYF_4$:Er,Yb microspinner so that its rotation speed can be determined by the analysis of the frequency spectrum (see **Figure 2d**). The optical force exerted on the microparticle has been measured by the hydrodynamic drag method. Optical forces have been found to increase linearly with the laser power as it was expected (see Supporting Information S4). It is important to remark here that, due to the non-spherical shape of the $NaYF_4$:Er,Yb microparticles, once they are optically trapped, the optical forces flip it to its vertical position (i.e. with its hexagonal face parallel to the laser beam propagation direction). [18]

When using the experimental set-up schematically drawn in Figure 2a the $NaYF_4$:Er,Yb microspinners are simultaneously trapped and rotated by the 790 nm radiation. Rotation is induced by the optical torque that, in turns, appears due to polarization change induced in the 790 nm laser radiation due to the optical birefringence of $NaYF_4$. The instantaneous optical torque (τ) per volume unit exerted over the microspinner as a function of the rotation angle (θ) can be written, in a first order approximation, as:

$$\tau = \frac{\Delta L}{\Delta t} \quad (1)$$

where ΔL is the angular momentum change per volume unit of the 790 laser radiation after passing through the microspinner. This is, in turn, proportional to the 790 nm laser power and to the optical birefringence of the material (Δn= 0.027 for the case of $NaYF_4$:Er,Yb). In steady-state conditions, the relation between the optical torque and the induced spinning velocity (Ω) is given by: [15b]

$$\Omega = \frac{\tau}{D} \quad (2)$$

where D is the drag coefficient that depends on the particle dimensions and geometry as well as on the medium viscosity. In a first order approximation, we can write:

$$D = B \cdot \eta \cdot R_{eff}^3 \quad (3)$$

B is a constant that depends on the particle geometry, η is the medium (water) viscosity and R_{eff} is the effective radius of the spinning particle. The effective radius is related to the volume of the spinning particle, V_{sp} by:

$$R_{eff} = \sqrt[3]{\frac{3 \cdot V_{sp}}{4 \cdot \pi}} \quad (4)$$

Thus, combining equations (1)-(4) we conclude that the spinning velocity, for a fixed laser power and material birefringence can be written as:

$$\Omega = \frac{A}{\eta \cdot V_{sp}} \quad (5)$$

where, again, A is a time independent constant that depends on the material birefringence, geometry and laser power. Expression (5) clearly indicates that any modification in the volume of the rotating particle or in the medium viscosity would have a direct impact in the spinning velocity. This is the basis of the single-attachment detection technique here proposed and schematically represented in **Figure 2c**. We state at this point that, for a fixed laser power, the rotation speed of a $NaYF_4$:Er,Yb UCSPN would be affected if its volume (or mass) changes as a consequence of the attachment of a single cell or bacterium. An attachment event increases the effective volume of the spinning particle, reducing its rotation velocity. In addition, we also state that when a single-cell or bacteria is in close proximity to the $NaYF_4$:Er,Yb microspinner it could affect the "effective medium viscosity" also leading to a change in the spinning velocity without the requirement of complete adhesion. The remarkable effect of single-cell adhesion in the rotation velocity of a $NaYF_4$:Er,Yb microspinner is evidenced in Figure 2d. It shows the frequency spectrum of a $NaYF_4$:Er,Yb microspinner before and after single cell adhesion (situations (ii) and (iii) of Figure 2c, respectively). Note that single-cell adhesion causes a noticeable reduction in the angular velocity (from 4.5π rad/s down to 0.5π rad/s). Thus, angular velocity becomes a highly sensitive indicator for real time, remote and contactless detection of adhesion events. At this point is important to note that the angular velocity depends, in a first order, only on the optical birefringence of the material. Therefore, the spinning velocity does not depend on the dopant and it will be the same in undoped particles. Then, $NaYF_4$ microparticles with other activators (including those leading to

down conversion emission) would be also perfectly suitable for optical driven spinning and, therefore, for single-cell detection. Also, other birefringent microparticles (such as $LiREF_4$ microparticles) could be used as spinners. [20]

The frequency spectrum of a optically rotated $NaYF_4$:Er,Yb microspinner included in Figure 2d were obtained by analyzing the time variations of the laser intensity registered by the quadrant detector. It is important to note here that an alternative approach to determine the rotation speed of a $NaYF_4$:Er,Yb microspinner is the analysis of its upconverting emission. As it has been discussed in detail in previous works, the upconversion emission spectra generated by a $NaYF_4$:Er,Yb particle is strongly polarized.[17-18] As a consequence, the shape of the upconverting emission spectrum depends on the relative orientation of the optical axis of the $NaYF_4$:Er,Yb particle (perpendicular to the hexagonal face) and the axis of the detection system (determined by a polarized laced at the entrance of the spectrometer). When a $NaYF_4$:Er,Yb particle is rotating with a fixed frequency the shape of the upconverting emission fluctuates in time with the same frequency.[18] Thus, the analysis of the spectral fluctuations of a $NaYF_4$:Er,Yb spinner can be also used to determine its rotation velocity. This possibility is demonstrated in **Figure 3**. Figure 3a shows the normalized upconverting spectra generated by a $NaYF_4$:Er,Yb UCSPN as obtained at different times. In this case we focus our attention to the $^4F_{9/2} \rightarrow {}^4I_{15/2}$ transition as it shows a high polarization degree.[18] Note that the particle rotation leads to a fluctuation in the ratio between the emitted intensities generated at 656 and 664 nm (I_{656} and I_{664}). Figure 3b shows the time evolution of the intensity ratio $R = I_{656}/I_{664}$ of an upconverting microspinner when optically trapped and rotated with a 100 mW laser beam. This intensity ratio presents a periodic fluctuation as indicating the rotation of the UCSPN with a well-defined angular velocity. Its rotation frequency can be determined from the frequency spectrum included in Figure 3c (close

to 2π rad/s in this particular case), which corresponds to the ratio fluctuations showed in Figure 3b. The frequency spectrum of the fluorescence fluctuations is, indeed, quite similar to that obtained from the analysis of the quadrant photodiode signal as it is evidenced in Figure 3c. Although both methods provide same results and are quite simple form an experimental point of view, the use of the quadrant photodiode signal seems to be more advantageous for the measurement of high spinning velocities. When using the polarized emission spectra for spinning velocity determination the maximum measurable velocity is, however, limited by the integration time required for the acquisition of the upconversion spectrum. Therefore, in this work we determined spinning velocities by using the quadrant photodiode signal.

We would like to remark that the fact that the spinners are up-converting nanoparticles is not necessary for single cell detection as the spinning velocity can be determined by using the time dependence of the scattering intensity of trapping beam. In this sense, luminescence is not necessary. Nevertheless, in this work it is demonstrated that the ability of our particles of generating upconversion luminescence is an additional feature that cannot only be used for the determination of spinning velocity but also to monitor the temperature during the biodetection event. Thus, upconversion emission is not strictly necessary for biodetection but provides extra-features of high interest such as remote thermal sensing.

2.3. Single-cell and single-bacteria detection.

As it has been explained in **Section 2.2**, the potential use of $NaYF_4$ UCSPNs for single body detection requires their surface modification to endow them with preferential attachment to targeted cells and bacteria. The possible influence of this surface decoration on the rotation dynamics of the $NaYF_4$ microspinners has been first evaluated by

measuring the spinning velocity versus laser power as obtained before and after surface decoration (see **Figure 4a**). As it can be observed, in both cases the spinning velocity increases linearly with the laser power, showing very similar trends. This, in turn, indicates that surface decoration has negligible impact neither in the effective radius of the UCSPN nor in its effective birefringence. In addition, we have also corroborated how the decoration process does not affect the two-photon luminescent properties of the UCSPN (see Supporting Information). We have also experimentally corroborated that, for a fixed laser power and in absence of either cells or bacteria in the medium, the spinning velocity is time independent either in the presence and absence of surface decoration (see **Figure 4b**). This indicates that, in our experimental conditions, the laser irradiation does not cause any remarkable change neither in medium viscosity nor in the particle's birefringence. This is a direct consequence of using 790 nm radiation that is not absorbed by the medium,[21] thus is leading to a negligible thermal loading. The absence of any relevant thermal loading was demonstrated by analyzing the green upconverting emission of the UCSPN for different laser powers. The green erbium emission is known to be highly temperature dependent as it is originating the thermally coupled $^{2}H_{11}$ and $^{4}S_{3/2}$ states.[11b] [22] Results included in **Figure 4c** and **Figure 4d** denote that, in our experimental conditions, the 790 nm laser-induced thermal loading of our UCSPN is not larger than 2 ºC in the whole range of laser powers used. This is opposite behavior to previous results using 980 nm laser radiation for optical rotation in which local thermal loading of several degrees was observed.[21]

For a single-cell detection, the surface decorated UCSPNs were placed in an aqueous solution containing *Candida albicans* cells. The UCSPN and cell concentration in the aqueous solution were set to be as low as 0.010 mg/ml and 0.005 mg/ml, respectively. The use of such low concentrations was mandatory to achieve single-particle trapping

and rotation as well as single-cell attachment events. **Figure 5a** shows the time evolution of the spinning velocity of a surface-decorated microspinner for a fixed laser power as obtained upon attachment and detachment of a *Candida albicans* cell. For the sake of a clear discussion we set $t = 0$ s when the presence of a *Candida albicans* starts to affect the spinning dynamics. During the 5 seconds before $t = 0$, the spinning velocity remains constant. Figure 5b.1 shows an optical image of the UCSPN in this time interval. No evidence of any cell close to the spinner is observed so that the cell-microspinner distance is, at least, larger than 5 μm. In these conditions, the UCSPN rotation velocity is determined by water viscosity that is time-independent. Between $t = 0$ and 5 seconds a *Candida albicans* cell approach the microspinner (it is at a distance below 5 microns, see Figure 5b.2). In this time interval, the spinning velocity of the UCSPN starts to decrease even before a physical contact appears with the cell. We state at this point that in this regime the presence of the cell increases the effective viscosity in the surroundings of the microspinner. This augmented "effective viscosity" originates from either the existence of cell-to-spinner collisions, which is not resulting in ultimate attachment, or from the appearance of a dynamic impedance due to the presence of the cell that disturbs the mass currents activated by the optical spinner. Independently of the particular cause, increasing the effective viscosity increases the drag force, leading to an angular deceleration. For times larger than 18 s, a physical cell-microspinner contact occurs and, due to the specific surface decoration of the spinner, cell and microspinner start to rotate together (see Figure 5b.3). The single-cell attachment causes a remarkable reduction in the angular velocity that, after complete attachment, remains constant. The cell-microspinner system finally rotates with an angular velocity close to 0.5π rad/s that constitutes a $\approx$ 6-fold reduction in respect of the angular velocity of the spinner before the single-cell attachment event. According to expression (5), this reduction can be explained in term of the increment of

the spinning volume. The volume of our UCSPN can be calculated from Figure 1a to be close to V_{spn}≈ 20 μm^3 whereas a single *Candida albicans* cell has an average volume of V_{cell} ≈ 88 μm^3. [23] Thus, cell- attachment increases the volume of the spinning system from 20 up to $V_{tot} = V_{cell} + V_{spn}$ ≈ 108 μm^3. This constitutes a ≈ 5.5-fold enlargement in the volume of the spinning system. Therefore, accordingly to expression (5), this 5.5-fold rise would lead to a 5.5-fold decrease in the spinning velocity. This is, indeed, very close to the 6-fold decrease observed experimentally. Thus, we state at this point that the angular deceleration is mainly caused by the increment in the effective volume of the microspinner-cell system. Nevertheless, other effects that are assumed constant when deriving expression (4), such as a reduction in the effective birefringence of the cell+UCSPN system, cannot be ignored.

It is expected that the change induced in the spinning velocity due to cell adhesion could be strongly dependent on the exact location of the attachment. We should note that, in our conditions, we have not control at all on the exact location of the cell-spinner attachment. When doing our experiments, several experiments were performed in the same conditions in order to check the reproducibility of the results as well as to evaluate whether or not there were remarkable case-to-case differences in the single-cell attachment event. We would like to mention at this point that the optical images included in Figure 5 were selected as the most representative ones. In other words, in majority of cases the cell-spinner attachment was produced at the side-wall (narrower side) of the spinner. It is difficult to explain why the cell was preferentially attached to this lateral wall but we can state that this is presumably due to larger surface of interaction, i.e. a higher density of protein-G in these lateral walls (a fact that was schematically indicated in Figure 1c). We also state that if cell attachment would be produced at different location (for instance at the largest hexagonal face) the reduction caused in the spinning velocity would be very

similar than when attaching to the lateral faces. This assertion is based on the fact that previous calculations demonstrate that, for the case of cell attachments, the reduction in the spinning velocity is well explained taking into account the increment in the effective volume caused by cell attachment. The increment in the effective volume of the spinner+cell system does depend only on the cell and particle volume and not on the particular location of cell attachment.

Figure 5b also shows the time evolution of the spinning velocity of a non-biofunctionalized UCSPN as obtained in exactly the same conditions and the data corresponding to a biofunctionalized spinner. In this case, the presence of a *Candida albicans* cell at distances shorter than 5 μm causes a slight reduction in the spinning velocity. Again we attribute this reduction to a decrease in the effective viscosity affecting the rotation dynamics of the $NaYF_4$:Er,Yb UCSPN. In this case, cell-UCSPN attachment does not take place and, very likely, favored by the currents caused by the UCSPN rotation, the *Candida albicans* cell is pushed away. Then, the initial spinning velocity is recovered.

The sensitivity of $NaYF_4$:Er,Yb UCSPNs was explored by testing their potential ability for single-body detection of much smaller biosystems. For this purpose the $NaYF_4$:Er,Yb UCSPNs were placed and optically rotated in an aqueous solution containing *Hafnia alvei* 1186 bacteria cells. The bacteria surface was modified to attach to surface-decorated NaYF4:Er,Yb UCSPNs as explained in Supporting Information. The time evolution of the rotation velocity of a surface decorated $NaYF_4$:Er,Yb UCSPN in presence of a single bacteria is included in **Figure 6a**. Again, $t = 0$ s is an arbitrary moment before the bacteria starts to affect the spinning dynamics. Before $t = 0$ s, the spinning velocity shows a time independent value close to 3π rad/s. At longer times single-bacteria appears in the

proximity of the $NaYF_4$:Er,Yb UCSPN. Due to its small dimensions, the bacteria is hardly seen by optical microscopy as it is evidenced in the optical pictures included in Figure 6b in which the bacteria location is indicated by the dashed circle. Bacteria-to-UCSPN attachment takes place in a very short time (less than 1 second). Once attachment is achieved, the spinning velocity decreases down to $\approx 2\pi$ rad/s, i.e. bacteria attachment leads to a 30% reduction in the spinning velocity. After the attachment event the $NaYF_4$:Er,Yb UCSPN rotates with a time-constant spinning velocity, this fact indicates the robustness of the attachment. Note that the bacteria attachment causes a reduction in spinning velocity much smaller than that produced by the *Candia albicans* cell attachment. This was, indeed, expected due to the much smaller dimensions of bacteria in respect to cells. On average, bacterium volume is estimated to be 0.6 μm^3 so that its attachment to the $NaYF_4$:Er,Yb UCSPN causes an increment in the total volume from 24 up to 24.6 μm^3, i.e. it causes an increment in the total volume as low as 3%. According to expression (5), this small increment in the total volume does not explain the 30 % reduction in the spinning velocity. We have to recall at this point, that expression (4) was derived assuming that the optical birefringence of the spinning system was not affected by the single-body attachment event. Nevertheless, this assumption could not be correct when dealing with bacteria attachment. *Hafnia alvei* bacterium body is a straight rod, 1.0 um in diameter and 2.0-5.0 um in length that could cause non-negligible shape-induced optical birefringence. In these conditions, the presence of a bacterium in physical contact with the $NaYF_4$:Er,Yb UCSPN could induce beam distortions as well as additional changes in the polarization state of laser radiations. These effects could result in a non-negligible modification in the effective birefringence of the bacteria+UCSPN system that, in turns, lead to a reduction in the spinning velocity larger than that expected from the volume increment itself. We, therefore, conclude that the dominant mechanism at the

basis of the angular deceleration caused by bacteria adhesion is the modification in the effective birefringence.

3. Conclusion

In conclusion, we present a very promising and fascinating tool for single cell (i.e. yeast or bacteria) detection, which circumvent the main drawback of the traditional techniques. It is based on real time determination of the rotation velocity of an optically trapped upconverting birefringent particle. In respect to conventional systems used for single-cell detection, the time response have been improved, as only a few seconds are needed to detect the presence of single-cells in the medium. In addition, the amount of sensing material required is minimum as, in its basic version, only one upconverting spinner is required for single-cell detection. Furthermore, straightforward analysis of upconversion luminescence provides the possibility of simultaneous real time thermal sensing, evidencing a negligible thermal loading in sensing experiments towards reproducibility of experimental conditions. The physical basis of single-cell and single-bacteria detection have been also discussed. While single-cell detection is related to the increment in the effective radius resulting in angular deceleration of UCSPN, the change in the effective birefringence seems to be responsible of the change in the rotation dynamics caused by single-bacteria attachment.

The experimental simplicity of the here proposed approach makes the system ready for miniaturization. Furthermore, the combination with already developed laser beam shaping techniques (e.g. diffraction optical elements) would allow for multiple optical trapping and rotation of several upconverting spinners [24], therefore, for development of multi-target bio-detection assays ‘panels’. The results included in this work open a new

avenue for the development of highly sensitive, fast and miniaturized systems for single cell detection that could overcome the limitations of systems being used nowadays.

Supporting Information

Supporting Information is available from the Wiley Online Library or from the author.

Acknowledgements

This work was partially supported by the Ministerio de Economía y Competitividad de España (MAT2016-75362-C3-1-R) and by the Instituto de Salud Carlos III (PI16/ 00812), by the Comunidad Autónoma de Madrid (B2017/BMD-3867RENIMCM), and co-financed by the European Structural and investment fond Additional funding was provided by COST action CM1403. D. Lu thanks the Chinese Scholarship Council for financial support. K.P. acknowledges the support from Foundation for Polish Science (FNP) under START program. A. B. acknowledges financial support from NCN OPUS DEC- 2017/27/B/ST7/01255 grant

Received: ((will be filled in by the editorial staff))

Revised: ((will be filled in by the editorial staff))

Published online: ((will be filled in by the editorial staff))

References

[1] a) K. S. Gracias; J. L. McKillip, *Canadian Journal of Microbiology*. **2004**, *50*,11, 883-890; b) R. T. Noble; S. B. Weisberg, *Journal of Water and Health.* **2005**, *3*,4, 381-392; c) L. Jimenez; S. Smalls; R. Ignar, *Journal of microbiological methods.* **2000**, *41*,3, 259-265.

[2] a) A. Krasnitz; J. Kendall; J. Alexander; D. Levy; M. Wigler, *Trends Mol Med.* **2017**, *23*,7, 594-603; b) A. R. Holmes; R. D. Cannon; M. G. Shepherd; H. F. Jenkinson, *J Clin Microbiol.* **1994**, *32*,1, 228-231.

[3] O. Lazcka; F. J. D. Campo; F. X. Muñoz, *Biosensors and Bioelectronics.* **2007**, *22*,7, 1205-1217.

[4] a) R. Etzioni; N. Urban; S. Ramsey; M. McIntosh; S. Schwartz; B. Reid; J. Radich; G. Anderson; L. Hartwell, *Nature Reviews Cancer.* **2003**, *3*,4, 243-252; b) J. T. Kaifi; G. Li; G. Clawson; E. T. Kimchi; K. F. Staveley-O'Carroll, *Cancer Biol Ther.* **2016**, *17*,8, 859-869.

[5] a) S. Tokonami; T. Iida, *Analytica Chimica Acta.* **2017**, *988*, 1-16; b) B. R. Panda; A. K. Singh; A. Ramesh; A. Chattopadhyay, *Langmuir.* **2008**, *24*,20, 11995-12000; c) S. Wu; N. Duan; Z. Shi; C. Fang; Z. Wang, *Analytical Chemistry.* **2014**, *86*,6, 3100-3107.

[6] a) X. Zhao; L. R. Hilliard; S. J. Mechery; Y. Wang; R. P. Bagwe; S. Jin; W. Tan, *Proceedings of the National Academy of Sciences of the United States of America.* **2004**, *101*,42, 15027-15032; b) F.-y. Su; Y. Endo; H. Saiki; X.-H. Xing; N. Ohmura, *Biosensors and Bioelectronics.* **2007**, *22*,11, 2500-2507; c) D. A. Boehm; P. A. Gottlieb; S. Z. Hua, *Sensors and Actuators B: Chemical.* **2007**, *126*,2, 508-514; d) F. Tang; D.-W. Pang; Z. Chen; J.-B. Shao; L.-H. Xiong; Y.-P. Xiang; Y. Xiong; K. Wu; H.-W. Ai; H. Zhang; X.-L. Zheng; J.-R. Lv; W.-Y. Liu; H.-B. Hu; H. Mei; Z. Zhang; H. Sun; Y. Xiang; Z.-Y. Sun, *Nanoscale.* **2016**, *8*,8, 4688-4698.

[7] a) D. Jaque; C. Richard; B. Viana; K. Soga; X. Liu; J. G. Solé, *Advances in Optics and Photonics.* **2016**, *8*,1; b) G. Mandl; D. Cooper; T. Hirsch; J. Seuntjens; J. A. Capobianco, *Methods and applications in fluorescence.* **2018**.

[8] a) N. Sanvicens; C. Pastells; N. Pascual; M. P. Marco, *TrAC Trends in Analytical Chemistry.* **2009**, *28*,11, 1243-1252; b) G. A. Sotiriou; S. E. Pratsinis, *Current Opinion in Chemical Engineering.* **2011**, *1*,1, 3-10.

[9] F. Auzel, *Journal of Luminescence.* **1990**, *45*,1, 341-345.

[10] a) D. K. Chatterjee; A. J. Rufaihah; Y. Zhang, *Biomaterials.* **2008**, *29*,7, 937-943; b) J. Xu; A. Gulzar; P. Yang; H. Bi; D. Yang; S. Gai; F. He; J. Lin; B. Xing; D. Jin, *Coordination Chemistry Reviews.* **2019**, *381*, 104-134; c) M. González-Béjar; L. Francés-Soriano; J. Pérez-Prieto, *Frontiers in Bioengineering and Biotechnology.* **2016**, *4*,47.

[11] a) K. Shin; Y. H. Song; Y. Goh; K. T. Lee, *Int J Mol Sci.* **2019**, *20*,6, 1424; b) F. Vetrone; R. Naccache; A. Zamarrón; A. Juarranz de la Fuente; F. Sanz-Rodríguez; L. Martinez Maestro; E. Martín Rodriguez; D. Jaque; J. García Solé; J. A. Capobianco, *ACS Nano.* **2010**, *4*,6, 3254-3258.

[12] a) P. Rodriguez-Sevilla; L. Labrador-Paez; D. Jaque; P. Haro-Gonzalez, *Journal of Materials Chemistry B.* **2017**, *5*,46, 9085-9101; b) M. Dienerowitz; M. Mazilu; K. Dholakia, *J Nanophotonics.* **2008**, *2*,1, 021875-021875; c) P. M. Bendix; L. Jauffred; K. Norregaard; L. B. Oddershede, *Ieee Journal of Selected Topics in Quantum Electronics.* **2014**, *20*,3.

[13] a) H. Zhang; K.-K. Liu, *Journal of The Royal Society Interface.* **2008**, *5*,24, 671-690; b) S. Drobczyński; K. Prorok; K. Tamarov; K. Duś-Szachniewicz; V.-P. Lehto; A. Bednarkiewicz, *ACS Photonics.* **2017**, *4*,8, 1993-2002.

[14] a) P. Galajda; P. Ormos, *Applied Physics Letters.* **2001**, *78*,2, 249-251; b) Z.-P. Luo; Y.-L. Sun; K.-N. An, *Applied Physics Letters.* **2000**, *76*,13, 1779-1781; c) N. B. Simpson; K. Dholakia; L. Allen; M. J. Padgett, *Opt Lett.* **1997**, *22*,1, 52-54.

[15] a) P. Chen; M. Song; E. Wu; B. Wu; J. Zhou; H. Zeng; X. Liu; J. Qiu, *Nanoscale.* **2015**, *7*,15, 6462-6466; b) P. Rodriguez-Sevilla; T. Lee; L. L. Liang; P. Haro-Gonzalez; G. Lifante; X. G. Liu; D. Jaque, *Advanced Optical Materials.* **2018**, *6*,12; c) P. Rodríguez-Sevilla; Y. Arita; X. Liu; D. Jaque; K. Dholakia, *ACS Photonics.* **2018**, *5*,9, 3772-3778.

[16] J. Suyver; J. Grimm; K. Krämer; H.-U. Güdel, *Journal of luminescence.* **2005**, *114*,1, 53-59.

[17] J. Zhou; G. Chen; E. Wu; G. Bi; B. Wu; Y. Teng; S. Zhou; J. Qiu, *Nano Letters.* **2013**, *13*,5, 2241-2246.

[18] P. Rodriguez-Sevilla; Y. Zhang; N. de Sousa; M. I. Marques; F. Sanz-Rodriguez; D. Jaque; X. Liu; P. Haro-Gonzalez, *Nano Letters.* **2016**, *16*,12, 8005-8014.

[19] U. Sjobring; L. Bjorck; W. Kastern, *Journal of Biological Chemistry.* **1991**, *266*,1, 399-405.

[20] P. Huang; W. Zheng; D. Tu; X. Shang; M. Zhang; R. Li; J. Xu; Y. Liu; X. Chen, *Advanced Science.* **2019**, *6*,10, 1802282.

[21] P. Haro-Gonzalez; W. T. Ramsay; L. Martinez Maestro; B. del Rosal; K. Santacruz-Gomez; M. del Carmen Iglesias-de la Cruz; F. Sanz-Rodriguez; J. Y. Chooi; P. Rodriguez Sevilla; M. Bettinelli; D. Choudhury; A. K. Kar; J. Garcia Sole; D. Jaque; L. Paterson, *Small.* **2013**, *9*,12, 2162-2170.

[22] A. Sedlmeier; D. E. Achatz; L. H. Fischer; H. H. Gorris; O. S. Wolfbeis, *Nanoscale.* **2012**, *4*,22, 7090-7096.

[23] F. M. Klis; C. G. d. Koster; S. Brul, *Eukaryotic Cell.* **2014**, *13*,1, 2-9.

[24] a) L. Paterson; M. P. MacDonald; J. Arlt; W. Dultz; H. Schmitzer; W. Sibbett; K. Dholakia, *Journal of Modern Optics.* **2003**, *50*,10, 1591-1599; b) D. Ott; S. Nader; S. Reihani; L. B. Oddershede, *Opt Express.* **2014**, *22*,19, 23661-23672.

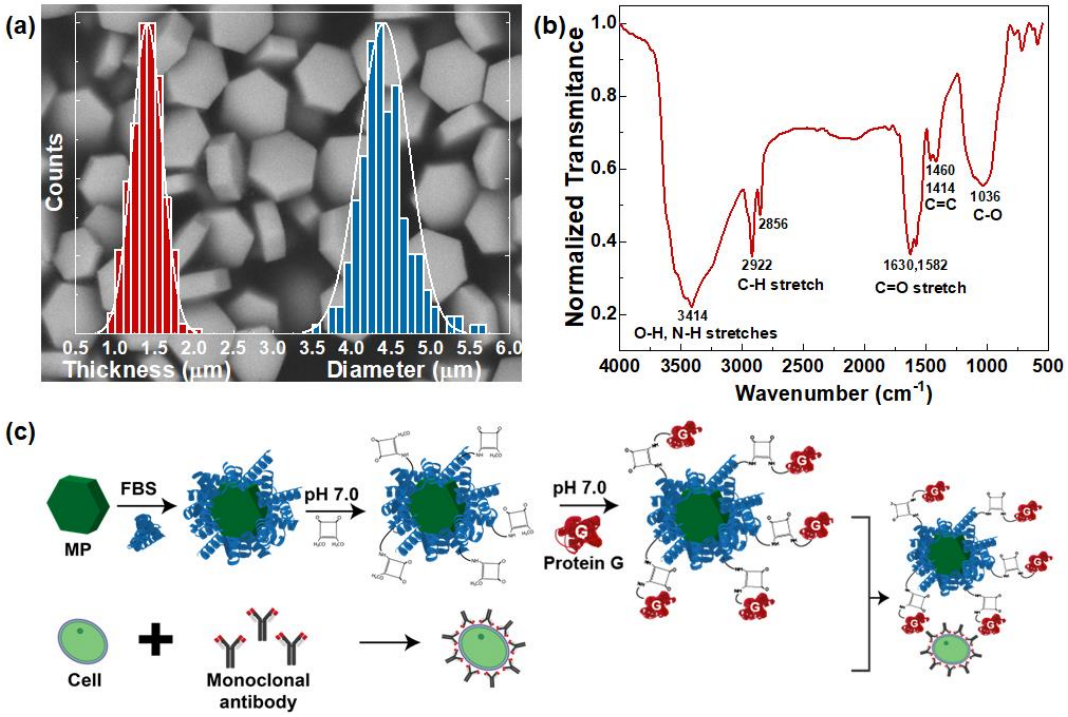

Figure 1.- (a) Scanning Electron Microscopy (SEM) image of the upconverting spinners used in this work, along with their diameter and thickness histograms obtained from the statistical analysis of SEM images. Average thickness and diameter of 1.4 ± 0.2 μm and 4.4 ± 0.3 μm are obtained, respectively. **(b)** FTIR of a concentrated sample of upconverting spinners used for single cell and single bacteria detection. **(c)** Schematic representation of the surface decorated upconverting spinner.

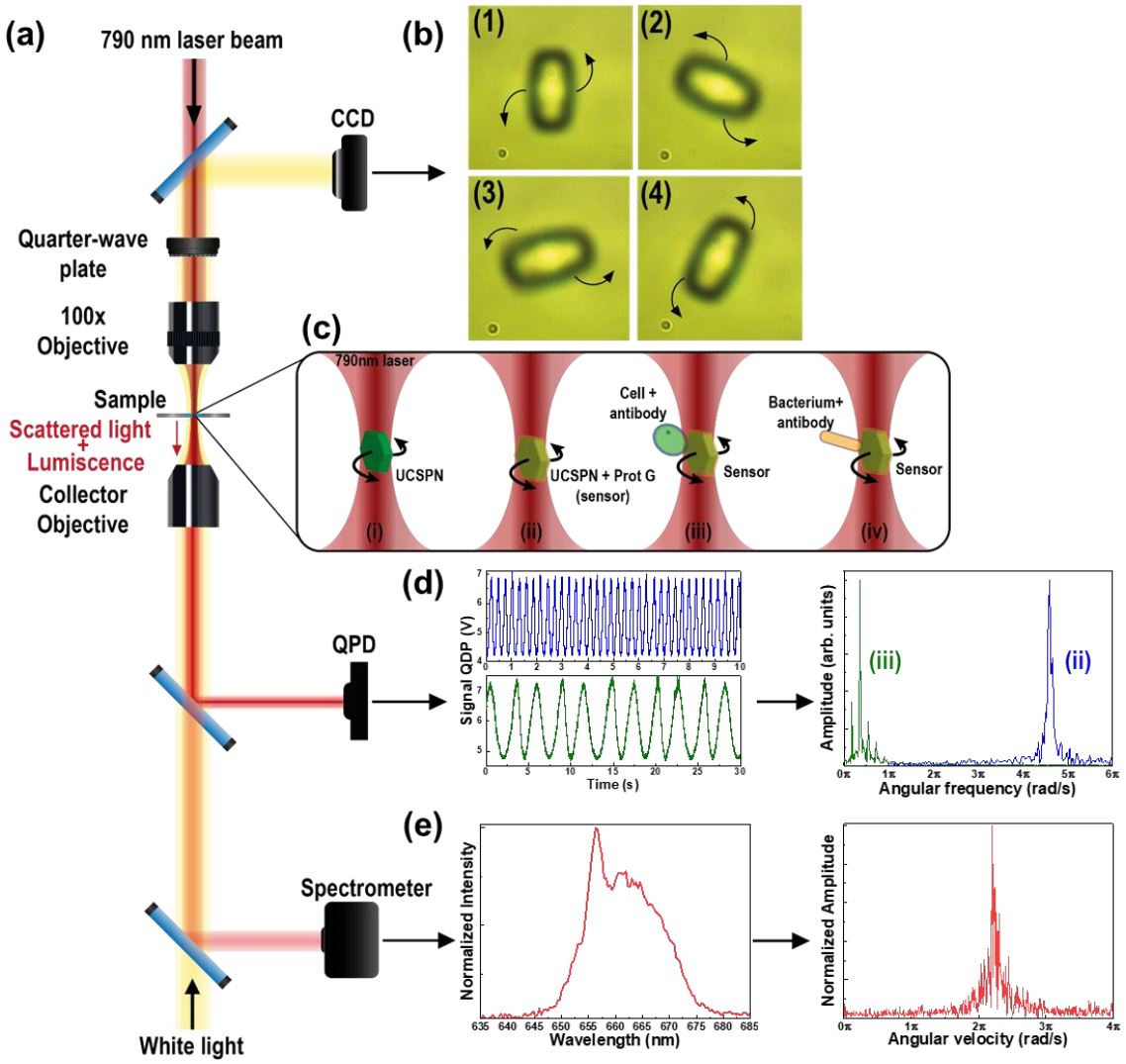

Figure 2.- (a) Schematic representation of the experimental set-up for optical trapping and rotation of UCSPN and single-body biodetection. The rotation speed of the UCSPN is determined by recording the intensity fluctuations of transmitted laser beam using a Quadrant PhotoDetector (QPD) or of polarized emission using a spectrometer, and by analyzing them in the frequency domain. Real time visualization of the UCSPN, bacteria and cells is possible thanks to the incorporation of a CCD camera. Some representative pictures of a UCSPN are included in **(b)**. The different situations evaluated all along this work are also schematically represented in **(c)**: trapping and rotation of a single and bare UCSPN (i), a surface functionalized UCSPN (ii), a surface functionalized UCSPN with an attached cell (iii), a surface functionalized UCSPN with an attached bacterium (iv). The attachment of either a bacterium or a cell to the optically rotating UCNP leads to a remarkable change in the rotation velocity that is quantified from the frequency spectrum. A representative example of the inducted change is also included in **(d)**. A typical upconversion luminescence spectrum acquired in our experimental conditions is included in **(e)** along with the frequency spectrum obtained from its ratiometric analysis and also used form for the determination of the angular velocity.

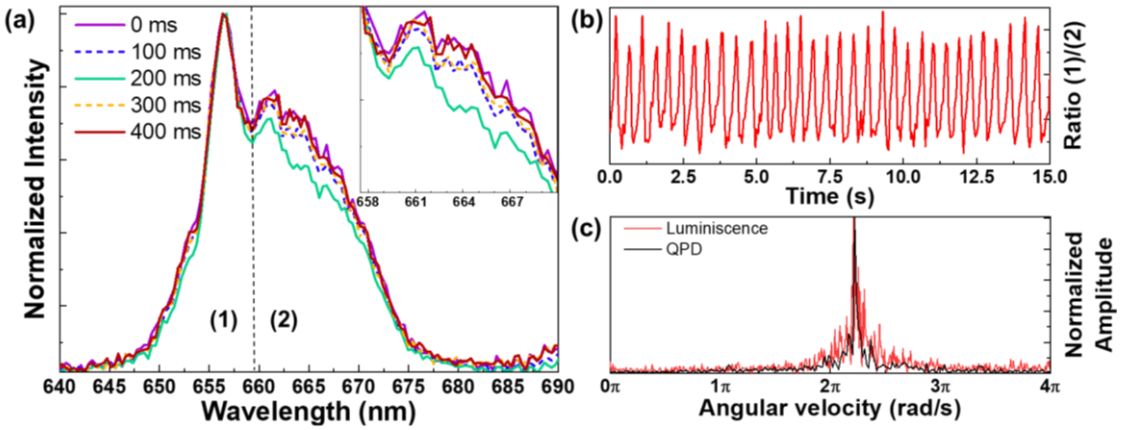

Figure 3.- (a) Polarized upconversion luminescence of a single rotated UCSPN, excited at 790 nm, where the intensity ratio between bands (1) and (2) presents a time dependence. Inset: Partially enlarged view of luminescence spectra. **(b)** Ratio fluctuations depending on time. **(c)** Angular velocity of a single UCSPN obtained by two different methods, from the intensity ratio fluctuations of the UCSPN polarized emission (red line) and from the intensity fluctuations of transmitted laser light using a Quadrant PhotoDetector (black line).

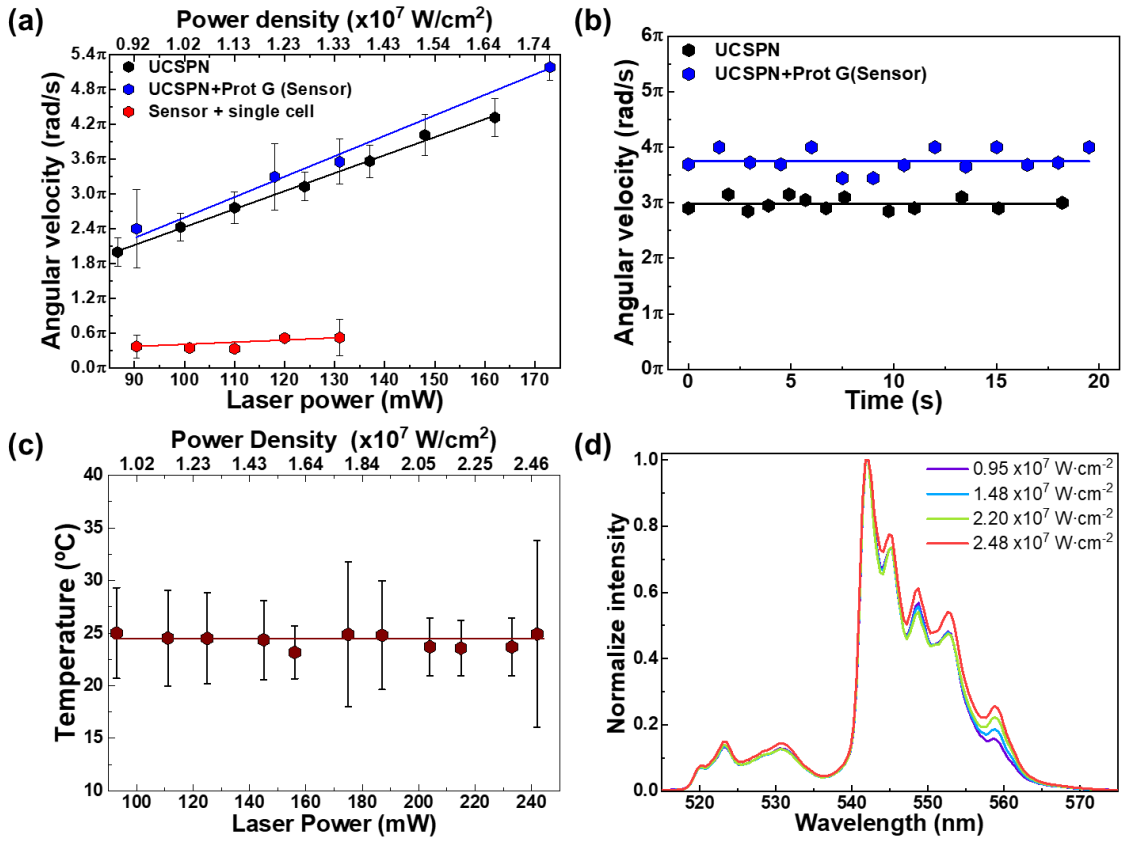

Figure 4. (a) Angular velocity as a function of the applied laser power and power density for a bare upconverting $NaYF_4:Er^{3+},Yb^{3+}$ microspinner (black line and hexagons) and for a microspinner decorated with Protein G, our sensor, (blue line and hex.) and a UCSPN+*Candida albicans* cell system (red line and hex.), optically trapped by a circularly polarized 790 nm laser beam. **(b)** Time-independent angular velocity of a single UCSPN optically trapped by a 790 nm laser beam at a fixed power. **(c)** Thermal loading of a UCSPN at different laser powers (and, therefore, power densities) as obtained from the analysis of the ratio between the Er^{3+} ions' emissions from the thermally coupled excited states $^4S_{3/2}$ and $^2H_{11/2}$ to the fundamental level $^4I_{15/2}$. The emission spectra from which temperature was evaluated are included in **(d).**

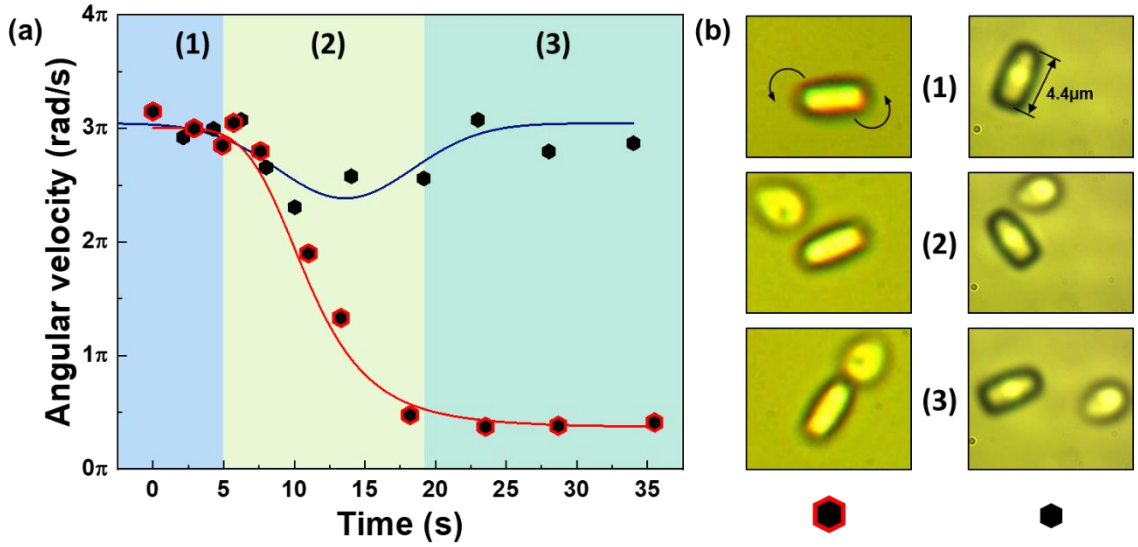

Figure 5. (a) Time evolution of rotation velocity of a surface functionalized UCSPN during the process of adhesion of a single cell. The control data, obtained with a non-functionalized UCSPN, is also shown for comparison. This control data have been obtained during the process of interaction between a single cell and the non-functionalized UCSPN. The cell-UCSPN friction produces a transient decrease in the angular velocity. **(b)** Sequential optical images of both functionalized and non-functionalized UCSPN as obtained when a cell circulates in their proximity. Note that effective cell adhesion is only observed for the surface functionalized UCSPN.

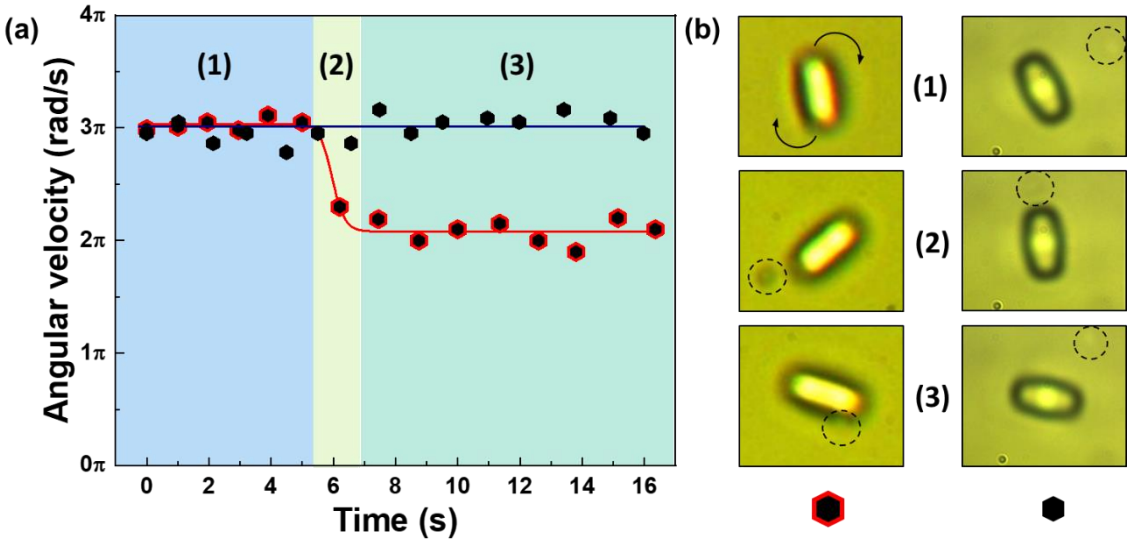

Figure 6.- (a) Time evolution of rotation velocity of a surface functionalized single UCSPN during the process of adhesion of a single bacterium. The control data, obtained with a non-functionalized UCSPN, is also shown for comparison. This control data has been obtained during the process of interaction between a single bacterium and the non-functionalized UCSPN. The bacterium-UCSPN friction produces a transient decrease in the angular velocity. **(b)** Sequential optical images of both functionalized and non-functionalized UCSPN obtained when a bacterium circulates in their proximity. Note, that bacterium adhesion is only observed for the surface functionalized UCSPN.

Supporting Information

Single-cell biodetection by upconverting microspinners

*Elisa Ortiz-Rivero[1], Katarzyna Prorok[2], Michal Skowicki[3], Dasheng Lu[1], Artur Bednarkiewicz[2] *, Daniel Jaque[1,4] * and Patricia Haro-González[1].*

S1. Materials and Synthesis of β-$NaYF_4$: 20% Yb^{3+}, 2% Er^{3+} microparticles

All of the chemical reagents in these experiments were used as received without further purification. Yttrium oxide (99.99%), ytterbium oxide (99.99%) and erbium oxide (99.99%) and sodium fluoride were purchased from ALDRICH Chemistry. Lanthanide nitrates were obtained by reactions stoichiometric amount of lanthanide oxides with nitric acid. Ethanol (96% pure p.a.), sodium citrate (pure p.a.) and nitric acid (pure p.a.) were purchased from Avantor (Poland). Fetal bovine serum (FBS) and 3,4-dimethoxy-3-cyclobutene-1,2-dione (99%) were purchased from Sigma Aldrich (St. Louis, MO, USA). Recombinant protein G was purchased from Thermo Scientific (Waltham, xMA, USA).

All chemicals were used as received without further purification. *Candia albicans* growth medium was composed of 1% bacto-peptone, 0.2% yeast extract, 0.2% casein hydrolysate, 2% glucose, 0.6% sodium chloride, and 1.2% agar (pH 7.6).

The $NaYF_4$ microparticles doped with 20 mol% Yb^{3+} and 2 mol% Er^{3+} ions were prepared using the hydrothermal method. Typically, aqueous solutions of sodium citrate (9.31 mL; 0.3 M) and $Ln(NO_3)_3$ (14 mL; 0.2 M; Ln = Y, Yb, Er) were mixed under vigorous stirring to form a milky suspension. Then, to beaker an aqueous solution of NaF (44.8 mL; 0.5 M) was added to form a transparent solution. The mixture was transferred to a 100-mL Teflon vessel and heated to 220 °C for 12 h. After cooling down to room temperature, the reaction product was isolated by centrifugation and washed with ethanol. Finally, the prepared particles were dispersed in water.

S2. Surface modification and functionalization of microparticles

Surface modification and functionalization has been performed according to modified method described in [1]. A water suspension (200 μL) of microparticles was added to 1 mL of 0.1 M HCl and vortexed for 10 min. The pellet was suspended in 200 μL dimethyl sulfoxide. The microparticles suspension was mixed with 1 mL of fetal bovine serum (FBS), incubated in an ultrasonic bath for 5 min, and incubated overnight on rotator. To separate the MPs from FBS, the sample was repeatedly centrifuged (5.000 g, 10 min, RT) and suspended in 0.9% NaCl containing 50 Mm 4-(2-hydroxyethyl)piperazine-1-ethanesulfonic acid (HEPES), pH 7.0. Protein G was crosslinked to the protein-capped MPs by squaric acid chemistry. First, 1 mg 3,4-dimethoxy-3-cyclobutene-1,2-dione was dissolved in saline and added to the microparticles suspended in 50 mM HEPES-buffered saline (HBS), pH 7.0. The suspension was vortexed for 1 h. After incubation, the samples were centrifuged (5,000 g, 10 min, RT) and suspended in 0.9% NaCl. This

step was performed 3 times. Upconverting microparticles were suspended in 1 mL of a 1 mg·mL^{-1} solution of protein G in 50 mM HBS, pH 9.0. This solution was vortexed for 1 h and purified by centrifugation (5.000 g, 10 min, RT) (3 times) and then suspended in 50 mM HBS, pH 7.0, and stored at 4 °C.

S3. Preparation of the samples

Microparticles coated with protein G (the denominated "upconverting Spinners", UCSPNs) tend to immobilize to the surface of the measurement chamber when suspended in water or buffered saline. Thus as a measurement buffer a 1% BSA in TBS (trizma buffered saline) has been used.

S4. Optical trapping and Optical forces measurement

The optical force exerted by a trapping laser beam on a single UCSPN dispersed in a fluid can be measure with the hydrodynamic method.[2] In this case, the optical force is compared to the known friction or drag force, opposed to the movement of the trapped UCSPN inside the fluid:

$$F_D = 6\pi\eta_{eff} R\, v \qquad \text{(S1)}$$

where η_{eff} is the effective viscosity of the medium, R is the microdisk radius and v is the escape velocity, the maximum velocity in which the UCSPN stays inside the trap.

To obtain the drag force, a linear controlled displacement between the trapped UCSPN and the medium was generated at a known constant velocity. The particle's displacement depend on the velocity value. When this velocity is low ($v < v_{esc}$), the displacement from the equilibrium position is small and the microdisk remains trapped. On the other hand, if the velocity is high ($v > v_{esc}$), the microdisk can be freed from the trap since the friction force overcomes the maximum optical force exerted on the trap's limit. The

hydrodynamic method consists on finding the escape velocity (v_{esc}) for different trapping laser powers. This velocity is the maximum velocity in which the microdisk stays inside the trap and the optical force is equal to the drag force. The hydrodynamic drag force as a function of the applied laser power is shown in **Figure S1**.

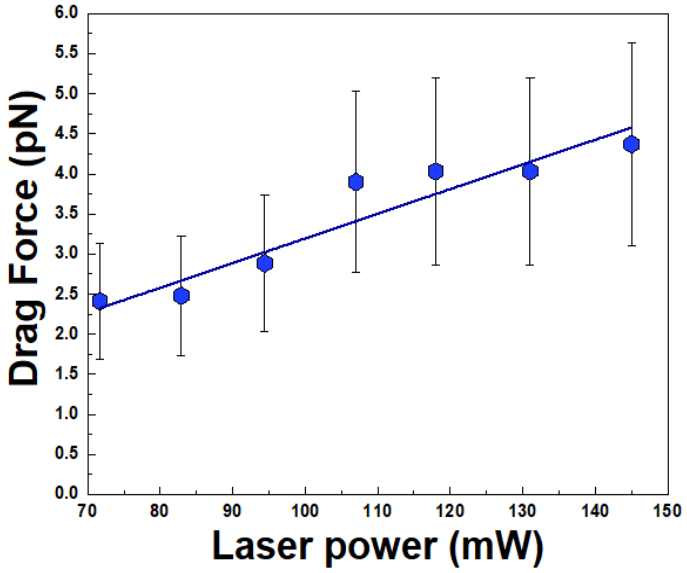

Figure S1. Hydrodynamic drag force as a function of the trapping laser power for a surface-decorated $NaYF_4$ microspinner.

S5. Optical properties of B-$NaYF_4$: 20% Yb^{3+}, 2% Er^{3+} microspinners

To characterize spectroscopically a single UCSPN, the emission spectra is obtained. An aqueous colloidal solution of UCSPN dispersion was placed in a confocal microscope. The excitation wavelength was provided by a 790 nm diode laser. The luminescence generated by a UCSPN was collected with the excitation objective and after passing through several pinholes and filters was spectrally analysed. The detection system comprises by a high sensitivity Si CCD camera (Synapse, Horiba) attached to a monochromator (iHR320, Horiba).

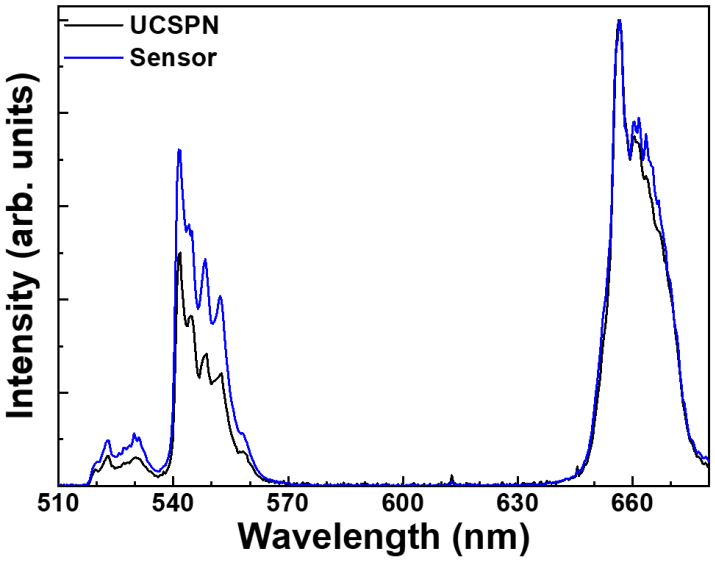

Figure S2 Emission spectra, excited at 790 nm, of a single UCSPN (black line) and our sensor, coated with protein G, (red line) normalized to the most intense transition.

S6. Statistics

The acquisition of the angular velocity vs laser power curves included in **Figure 4a** is complemented with measurements performed using different particles for each case (bare UCSPNs, biofunctionalized UCSPNs and UCSPNs+*Candida albicans* cell systems), for each point up to n = 5, as it is depicted in **Figure S3**. The displayed value is the average value obtained in each case and the error bars are the standard deviation of each set of measurements.

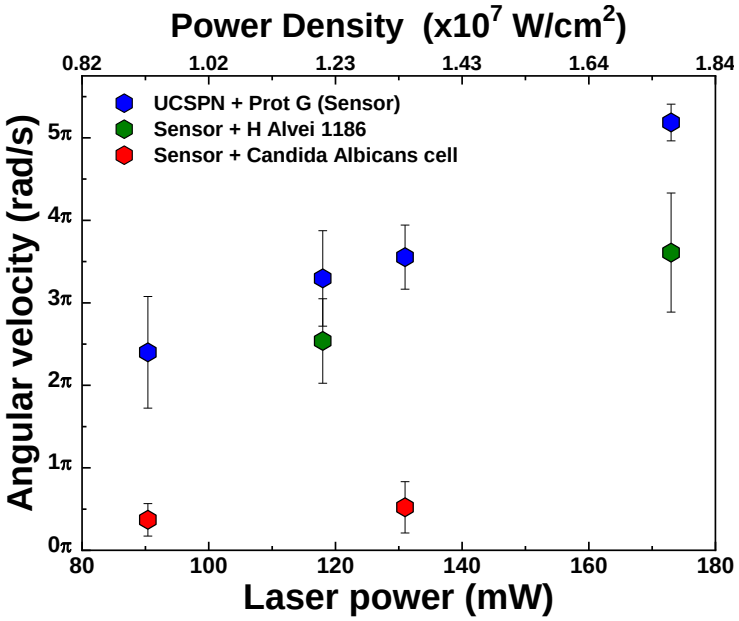

Figure S3. Statistic measurements at different laser powers of single bacteria detectors, UCSPNs, (blue hexagons), UCSPNs with bacteria attached (green hex.) and UCSPNs with a single cell attached (red hex.).

REFERENCES SUPPORTING INFORMATION

[1] M. Misiak; M. Skowicki; T. Lipiński; A. Kowalczyk; K. Prorok; S. Arabasz; A. Bednarkiewicz, *Nano Research.* **2017**, *10*,10, 3333-3345.

[2] P. Rodríguez-Sevilla; K. Prorok; A. Bednarkiewicz; M. I. Marqués; A. García-Martín; J. García Solé; P. Haro-González; D. Jaque, *Nano Letters.* **2018**, *18*,1, 602-609.